

RESEARCH ARTICLE

The Rho signalling pathway mediates the pathogenicity of AHPND-causing *V. parahaemolyticus* in shrimp

Tze Hann Ng¹  | Chia-Wei Lu² | Shih-Shun Lin³ | Che-Chih Chang¹ | Loc H. Tran^{4,5} | Wen-Chi Chang⁶ | Chu-Fang Lo^{1,2} | Han-Ching Wang^{1,2} 

¹Department of Biotechnology and Bioindustry Sciences, College of Biosciences and Biotechnology, National Cheng Kung University, Tainan, Taiwan

²International Center for the Scientific Development of Shrimp Aquaculture, National Cheng Kung University, Tainan 701, Taiwan

³Institute of Biotechnology, National Taiwan University, Taipei, Taiwan

⁴Department of Aquaculture Pathology, College of Fisheries, Nong Lam University, Ho Chi Minh City, Vietnam

⁵ShrimpVet Laboratory, Nong Lam University, Ho Chi Minh City, Vietnam

⁶Institute of Tropical Plant Sciences, College of Biosciences and Biotechnology, National Cheng Kung University, Tainan, Taiwan

Correspondence

Han-Ching Wang, Department of Biotechnology and Bioindustry Sciences, College of Biosciences and Biotechnology, National Cheng Kung University, Tainan 701, Taiwan.

Email: wanghc@mail.ncku.edu.tw

Funding information

Ministry of Science and Technology, Grant/Award Numbers: MOST 106-2313-B-006-007-MY3 and MOST 106-2633-B-006-004

Abstract

An emerging bacterial disease, acute hepatopancreatic necrosis disease (AHPND), is caused by strains of *Vibrio parahaemolyticus* with an additional AHPND-associated plasmid pVA1 encoding a virulent toxin (Pir^{VP}) that damages the shrimp's hepatopancreas. Like other species of *Vibrio*, these virulent strains initially colonise the shrimp's stomach, but it is not yet understood how the bacteria or toxins are subsequently able to cross the epithelial barrier and reach the hepatopancreas. Here, by using transcriptomics and system biology methods, we investigate AHPND-induced changes in the stomach of AHPND-causing *V. parahaemolyticus* (5HP)-infected shrimp and identify host molecular mechanisms that might explain how the integrity of the stomach barrier is compromised. We found that the expression of 376 unique genes was differentially regulated by AHPND infection. Gene ontology, protein interaction, and gene-to-gene correlation expression interaction analyses indicated that in addition to the immune system, a number of these genes were involved in cytoskeleton regulation by Rho GTPase. The involvement of Rho pathway regulation during AHPND pathogenesis was further supported by experiments showing that while Rho inhibitor pretreatment delayed the infection, pretreatment with Rho activator enhanced the pathogenicity of 5HP, and both the bacteria and toxin were detected sooner in the hepatopancreas. Further, disruption of the stomach epithelial structure was found in both Rho preactivated shrimp and in 5HP-infected shrimp. Taken together, we interpret our results to mean that Rho signalling helps to mediate AHPND pathogenesis in shrimp.

KEYWORDS

AHPND, Rho signalling, shrimp, *Vibrio parahaemolyticus*

1 | INTRODUCTION

After the first outbreak of a newly emergent shrimp disease, acute hepatopancreatic necrosis disease (AHPND), in 2009, the causative agent was subsequently identified as a virulent strain of *Vibrio parahaemolyticus* (Tran et al., 2013). AHPND-causing *V. parahaemolyticus* (5HP) was shown to have an additional extrachromosomal plasmid that was not present in the non-AHPND-causing *V. parahaemolyticus* (S02; Han, Tang, Tran, & Lightner, 2015; Kondo et al., 2014; Yang et al., 2014). This extrachromosomal plasmid encodes

a homologue of the insecticidal *Photobacterium* insect-related (Pir) binary toxin, and this Pir homologue (Pir^{VP}) acts as a pore-forming toxin that kills cells and induces AHPND in shrimp (Han et al., 2015; Lee et al., 2015). The symptoms of AHPND include a pale hepatopancreas and empty gut, and a particular characteristic is the sloughing of the epithelial cells of the hepatopancreas tubule and massive hemocytic infiltration, both of which can be observed under histological examination (Lai et al., 2015; Tran et al., 2013). It has been established that strains of *V. parahaemolyticus*, which contain the AHPND-associated plasmid without the *pir*^{VP} genes, fail to induce AHPND in shrimp.

In the early stage of an acute infection, 5HP initially colonises and replicates in the stomach, and only later (~6 hr post immersion [hpi]) appears in the hepatopancreas (Lai et al., 2015). It is only during this later stage that a strong inflammatory response and melanization can be observed in the hepatopancreas tubules (Soto-Rodriguez, Gomez-Gil, Lozano-Olvera, Betancourt-Lozano, & Morales-Covarrubias, 2015). In the course of the disease, high-throughput transcriptomic analysis has already shown that many immune-related genes are differentially expressed in the stomach, hepatopancreas, and intestine of AHPND-infected shrimp (Ge et al., 2017; Soonthornchai et al., 2016). However, it is not clear how these immune responses might allow 5HP to penetrate the shrimp gastrointestinal barriers to reach the hepatopancreas. Curiously, it has been shown that although recombinant PirB^{vp} toxin was able to produce AHPND-like histological signs by direct application via reverse gavage, the same toxin failed to cause any damage when introduced per os by feeding (Lee et al., 2015). This result suggested that there may be specific molecular pathway(s) in shrimp stomachs that need to be triggered by 5HP in order to allow the pathogenesis of the disease to proceed. In an effort to identify which specific molecular pathway(s) might be triggered during 5HP infection, in this study, we use a transcriptomics approach to investigate AHPND-induced changes in shrimp stomach gene expression level that are unique between 5HP- and S02-infected shrimp. Our results show that the cytoskeleton regulation Rho GTPase pathway was differentially regulated. We present further evidence from animal experiments and histological observations that support our proposal that the Rho signalling pathway may therefore be involved in AHPND pathogenesis in shrimp.

2 | RESULTS

2.1 | PCR detection of the *pirB^{vp}* sequence in the stomach of shrimp challenged with *V. parahaemolyticus*

Challenge tests were conducted with three groups of shrimp that were respectively immersed in the bacterial strains S02 (non-AHPND-causing strain) or 5HP (AHPND-causing strain) or in the tryptic soy broth (TSB) control. Shrimp stomachs were collected individually at the two indicated time points (Figure S1a). Total DNA was extracted from the stomachs, and the *pirB^{vp}* sequence was detected by PCR with the Pir primer set shown in Table S1. At 24 hpi, three of the shrimp infected with 5HP gave positive PCR results, whereas the other two shrimp gave negative PCR results (Figure S1b). At 1 wpi, *pirB^{vp}* was not detected in any of the surviving shrimp that were challenged with 5HP (Figure S1b). There were no positive PCR results for any shrimp immersed in the S02 or TSB controls at 24 hpi or at 1 wpi.

2.2 | Whole-transcriptome analysis and annotations

The transcriptome analysis used stomach samples collected at 24 hpi (TSB, *n* = 3; S02, *n* = 3; and 5HP, *n* = 5) and 1 wpi (TSB, *n* = 3; S02, *n* = 3; and 5HP, *n* = 3); that is, the analysis used all five of the 24 hpi stomach RNA samples from the 5HP group, but only the three samples that were best in terms of quality from all the other groups and sampling times. An average of ~18 million reads were generated

per sample (Table S2). After the removal of the low-quality reads, the remaining paired reads from all the samples were combined for de novo assembly, and 355,149 contigs were successfully assembled (Table S3). These contigs were then used as input to three separate platforms, PANTHER, ContigViews, and EXPath.

2.3 | Acute hepatopancreatic necrosis disease gene expression signature

Infection-induced changes in gene expression are known to be different between pathogenic and nonpathogenic *V. parahaemolyticus* (Wang et al., 2015). We therefore sought to identify the AHPND-induced changes in gene expression between 5HP and S02 strains. By using the PANTHER platform to run The Basic Local Alignment Search Tool (BLAST) on the Flybase database, 40,046 of the 355,149 assembled contigs were matched to defined *Drosophila melanogaster* genes. In the 24 hpi shrimp stomach samples, 36,988 of these contigs were found in the TSB samples, 37,052 of these contigs were found in the S02 samples, and 36,698 of these contigs were found in the three *pirB^{vp}*-positive 5HP samples (Figure 1a). (For convenience, these three *pirB^{vp}*-positive samples are subsequently referred to as the 5HP-P group.) From these defined contigs, we identified 376 differentially expressed genes (Table S4) that were affected by 5HP-P challenge but not by S02 challenge. We hypothesize that the differential expression of at least some of these 376 genes by 5HP-P may contribute to AHPND pathogenesis in infected shrimp.

2.4 | Functional classification of proteins and pathways regulated during AHPND infection

To investigate the biological functions of the 376 genes that had altered expression levels during infection in 5HP-P shrimp, the PANTHER functional classification tool was used to categorise these genes by molecular function, biological process, protein class, and cellular pathways. The results of this GO analysis are shown in Figure 1b. In terms of protein class, nucleic acid-binding proteins made up the largest single class of affected genes. In terms of the molecular function, approximately half of the 376 genes were involved in catalytic activity, with most of these being enzyme proteins (i.e., oxidoreductase, hydrolase, transferase, ligase, and lyase). Metabolic processes and cellular processes accounted for about two thirds of the biological processes. In terms of the pathway classification (Figure 1c), both cytoskeleton regulation and an inflammation pathway were well represented.

2.5 | Gene-to-gene correlation networks during AHPND infection

In parallel with the above gene expression analysis, we also used ContigViews to construct a gene-to-gene expression correlation network. For annotation, BLAST was used to compare the 355,149 assembled contigs first with the NCBI-PM database and then, if no hit was found, with the EMBL CDS database. The reference ORF sequence from the best Blast hit was then used to align with the predicted amino acids of the contig for ORF verification. For further gene

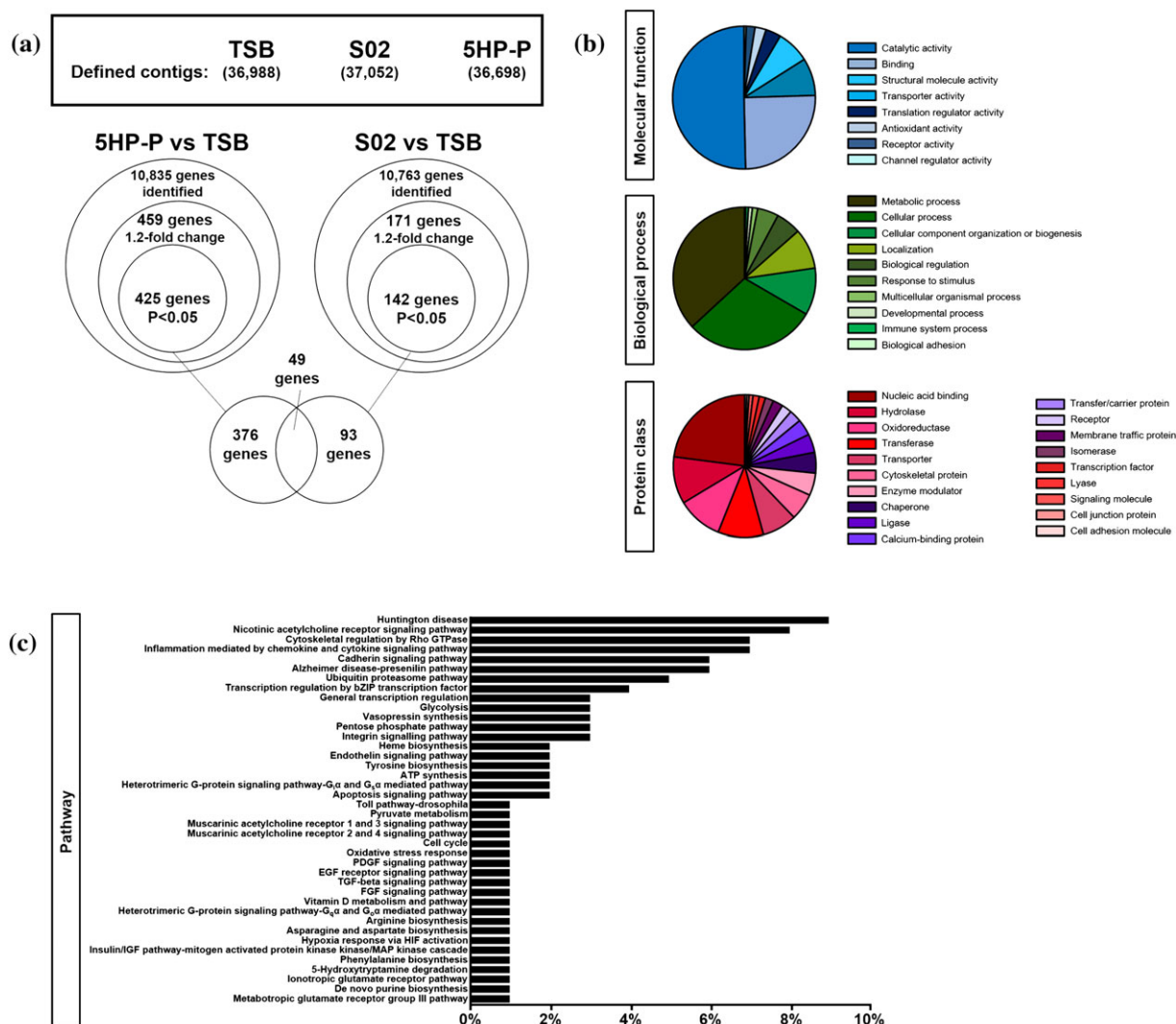


FIGURE 1 Functional classification of differentially expressed genes (DEGs) during acute hepatopancreatic necrosis disease (AHPND). (a) Representation of how transcriptomics data were processed to identify the differentially regulated genes affected by AHPND. To compare the *pirB*^{VP}-positive (5HP-P) and tryptic soy broth (TSB) shrimp at 24 hr post immersion, a list was made of every gene that occurred in at least one of the 5HP-P or TSB samples with FPKM expression >10. From this list of 10,835 genes, 425 genes further satisfied both criteria of a 1.2-fold change and p value <0.05. To determine the extent to which non-AHPND *V. parahaemolyticus* also affected the same genes, we repeated the same process for the non-AHPND-causing *V. parahaemolyticus* (S02) and TSB groups. After eliminating 49 genes that were differentially regulated the same way in both groups, there remained 376 unique genes whose expression levels were altered during AHPND infection. (b) Pie charts depicting the functional classification of DEGs found in the 5HP-P group. The DEGs were characterized using gene ontology (GO) analysis. Subcellular and functional categories were based on the GO annotations using the PANTHER Classification System for the categories of biological process, molecular function, and protein class. (c) Functional classification of the same DEGs according to their associated pathways. bZIP = basic leucine zipper; EGF = epidermal growth factor; FGF = fibroblast growth factor; HIF = hypoxia-inducible factor; MAP = mitogen-activated protein; PDGF = platelet-derived growth factor

ontology (GO) analysis, 37,678 defined contigs were identified and subjected to Blast2GO software (Table S3). The next step was to conduct a one-by-one comparison to identify genes that had ≥ 2 -fold expression changes between each of the three 5HP-P shrimp and each of the three S02 shrimp. For each of the resulting nine lists, every gene with a correlation coefficient of ≥ 0.95 (or ≤ -0.95) was included in an expression correlation network analysis. On the basis of these analyses, each gene was ranked according to the number of its connections, with only the top 100 genes from each list being considered. Thus, 900 genes with positive correlation and 900 genes with negative correlation were selected. In a final refinement step, only genes, which appeared in at least eight of the nine lists, were used to

construct the correlation network shown in Figure 2. Of the 23 genes in this network, 16 had lower expression level in the 5HP-P group and 7 had higher expression levels (Table S5). We also note that seven of these genes are related to immunity and seven others are related to the Rho signalling pathway (Table 1).

To validate the transcriptomics data, stomach samples were subjected to real-time reverse transcription polymerase chain reaction to measure the gene expression of four genes with higher expression in the S02 group and four genes with higher expression in the 5HP-P group. Five of these genes were Rho related, and the other three were related to immunity. We found that the real-time reverse transcription polymerase chain reaction results for all of these genes were

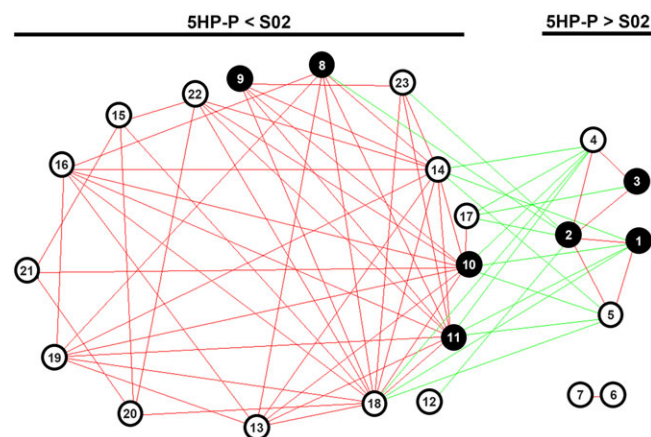


FIGURE 2 Gene-to-gene correlation network of genes that were most highly implicated in the pathogenesis of acute hepatopancreatic necrosis disease (AHPND) induced by AHPND-causing *Vibrio parahaemolyticus* (5HP). Genes with ≥ 2 -fold expression change between the non-AHPND-causing *V. parahaemolyticus* (S02; $n = 3$) and *pirB*^{VP}-positive 5HP (5HP-P; $n = 3$) groups were selected for network analysis, with only highly correlated genes that appeared in at least eight comparison groups being used to construct this relationship map. A positive correlation between two genes is indicated by a red line, whereas a negative correlation is indicated by a green line. The numbers in the circles correspond to the contigs in Table 1. Genes related to Rho signalling are indicated by the black circles

consistent with the expression pattern produced by the transcriptomics analysis (Figure S2).

2.6 | Changes in the Rho pathway during AHPND pathogenesis

While noting that the activation/inactivation of the Rho signalling pathway is based on the catalytic activity of the small GTP-binding proteins (GTPases) and the phosphorylation status of downstream effectors (Schwartz, 2004), we mapped our transcriptome database to KEGG in order to show changes in the actin cytoskeleton pathway (Figure S3 and Table S6). Most of the downstream genes in the regulation pathway were not changed; however, Rho guanine nucleotide exchange factor (RhoGEF), a regulatory factor that activates Rho GTPase, was upregulated in the 5HP-P shrimp samples. To investigate whether the Rho pathway is activated after AHPND infection, we used RhoA G-LISA activation assay kit to measure the RhoA activation levels in shrimp that had been challenged with the AHPND-causing strain 5HP. Figure 3a shows that RhoA was activated in shrimp with 5HP infection compared with the TSB control group. Meanwhile, ultrastructural observation of the anterior midgut epithelium by transmission electron microscopy (TEM) shows that the TSB-treated shrimp had much more regularly distributed vacuoles in the cell cytoplasm and well-organised microvilli (Figure 3b, A and B). By contrast, in the 5HP-infected shrimp, there was an accumulation of vacuoles at the apical side of the epithelial cells, while both cell lysis and disorganised microvilli were observed (Figure 3b, C–E). Widened cell junctions between adjacent cells were also observed in 5HP-infected shrimp (Figure 3b, E). Measurements showed that the junction gaps in 5HP-infected shrimp were

TABLE 1 Major genes that are involved in or correlated with AHPND pathogenesis

| Contig | Gene annotation | Rho signalling related | Immune related |
|--------------|--|------------------------|----------------|
| 5HP-P > S02 | | | |
| PVHP134552.2 | Rho GTPase-activating protein | ☑ | |
| PVHP256849.1 | NAD ⁺ ADP-ribosyltransferase | ☑ | |
| PVHP256096.1 | Arrestin | ☑ | ☑ |
| PVHP138073.1 | Peritrophin (chitin-binding peritrophin-A domain) | | ☑ |
| PVHP267995.5 | Ileal sodium/bile acid cotransporter | | |
| PVHP267311.2 | Undefined gene | | |
| PVHP194171.1 | Undefined gene | | |
| 5HP-P < S02 | | | |
| PVHP273473.1 | Tetraspanin-like protein | ☑ | |
| PVHP207640.1 | Class B secretin-like G-protein coupled receptor (GPRmth1) | ☑ | |
| PVHP40072.2 | Putative allatostatin C | ☑ | |
| PVHP178917.1 | Radixin, moesin | ☑ | |
| PVHP203414.1 | UNC93-like | | ☑ |
| PVHP82081.2 | Prophenoloxidase-activating enzyme | | ☑ |
| PVHP72255.1 | HHAP | | ☑ |
| PVHP237481.2 | Chitin synthase | | ☑ |
| PVHP237480.1 | Chitin synthase variant | | ☑ |
| PVHP173874.1 | DNA-directed RNA polymerase I–III subunit | | |
| PVHP295795.3 | Glutamate carboxypeptidase II-like | | |
| PVHP162239.1 | Methyltransferase-like protein 7A | | |
| PVHP157499.4 | Beta-1,4-N-acetylgalactosaminyl transferase | | |
| PVHP295792.1 | Glutamate carboxypeptidase 2-like | | |
| PVHP132943.1 | Nuclear transcription factor | | |
| PVHP271238.1 | Undefined gene | | |

Note. 5HP-P = *pirB*^{VP}-positive shrimp; AHPND = acute hepatopancreatic necrosis disease; HHAP = hemocyte homeostasis-associated protein.

significant wider than in the TSB-treated shrimp ($p < .05$; Figure 3c), suggesting that there is a loss of midgut barrier integrity in the 5HP-infected shrimp.

To confirm the involvement of the Rho pathway in AHPND pathogenesis, Rho Activator II (Cytoskeleton Inc.) was used to preactivate this pathway prior to AHPND infection. As before, activation was monitored by the RhoA G-LISA activation assay. Figure 4a shows that RhoA was activated 2 hr after Rho activator pretreatment. At 3 hr post-AHPND infection, we found that both Rho activator pretreatment and 5HP infection led to higher levels of RhoA activation compared with the S02-infected shrimp (Figure 4b). However, at 6 hpi, the higher level of activation was

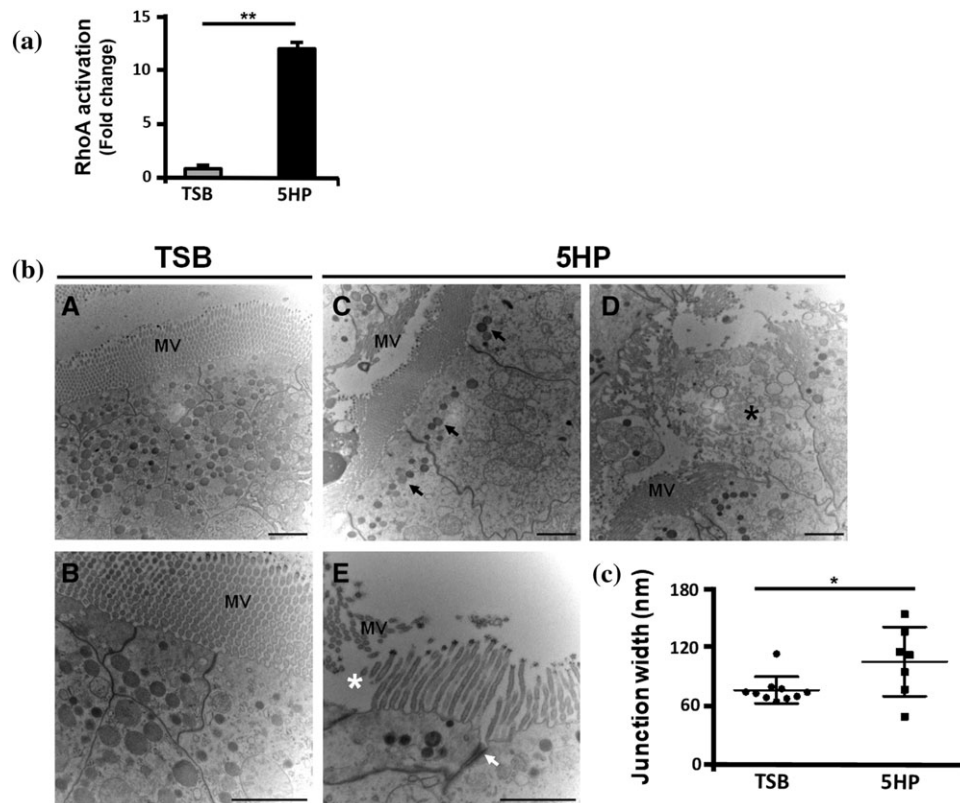


FIGURE 3 Effects of acute hepatopancreatic necrosis disease (AHPND) infection on Rho activation and anterior midgut epithelium structure. (a) Shrimp were challenged by immersion in AHPND-causing *V. parahaemolyticus* (5HP) strain or in tryptic soy broth (TSB) controls. Shrimp stomachs were taken from each group at 3 hr after infection. Rho activation was measured using the RhoA G-LISA activation assay. Statistically significant differences were determined by unpaired Student's *t* test ($^{**}p < .005$). (b) transmission electron microscopy observation of anterior midgut epithelium ultrastructure showing (A,B) well-organised microvilli (MV) and even distribution of vacuoles in the cytoplasm of epithelial cells in TSB-treated shrimp. (C) In 5HP-infected shrimp, vacuoles accumulated at the apical side of the epithelial cells (black arrows). Damage to the epithelial cells' integrity included (D) a lysed cell (asterisk), (E) disorganised microvilli, and a wider cell-cell junction between adjacent cells (white arrow). Scale bar: 2 μ m. (c) The width of the cell junction gap in TSB-treated and 5HP-infected shrimp. Statistically significant differences were determined by unpaired Student's *t* test ($^{*}p < .05$)

only found in the 5HP-infected shrimp with Rho activator pretreatment (Figure 4b). We also found that preactivation of Rho significantly enhanced the mortality of shrimp infected with 5HP ($p < .05$; Figure 5a), whereas pretreatment with Rho Inhibitor I (Cytoskeleton Inc.) significantly reduced mortality in 5HP-challenged shrimp ($p < .0001$; Figure 5b). At 3 hpi, hepatopancreas epithelium necrosis was observed in some of the 5HP-infected groups, whereas hemocytic infiltration, a marker of the late phase of AHPND, was only observed in 5HP-infected groups with Rho preactivation (Figure 6a and Table 2). Conversely, after Rho inhibition, between 3 and 12 hpi, epithelium necrosis was seen in only one of the 5HP-challenged groups (Figure 6b and Table 3).

Previous studies have shown that AHPND-causing bacteria are detected in shrimp stomach first and only subsequently in the hepatopancreas (Lai et al., 2015), and it seems likely that the Rho pathway might be involved in this transmigration from the stomach to the hepatopancreas. To investigate this possibility, we investigated how Rho preactivation affected the number of AHPND-causing bacteria in the stomach and hepatopancreas of challenged shrimp. In 5HP-infected shrimp, we found that Rho preactivation appeared to accelerate the migration such that the number of bacteria in the hepatopancreas peaked at 3 hpi as compared with 6 hpi without

pretreatment (Figure 7a). Rho preactivation also induced higher expression levels of *pirB^{vp}* mRNA in both the stomach and hepatopancreas of 5HP-infected shrimp (Figure 7b). Finally, we also observed that after Rho preactivation, some of the TSB control shrimp showed a loss of integrity of the brush border in the midgut epithelium (compare Figure 7c, A vs. B). Similarly damage to the brush border was also seen in some of the shrimp that were challenged with 5HP but not with any of the S02-infected shrimp (compare Figure 7c, G vs. C–E). We note, however, that even within a given experiment group, results were not always consistent. For example, not all of the 5HP-infected shrimp showed a loss of brush border integrity at 3 hpi. These differences may be due to individual variation and/or a relatively low bacterial load in a particular individual shrimp.

3 | DISCUSSION

Previous studies have shown that immune-related genes such as penaeidins, crustin, and anti-lipopolysaccharide factor were greatly altered during AHPND infection (Ge et al., 2017; Soonthornchai et al., 2016; Visetnan, Supungul, Tassanakajon, Donpudsa, &

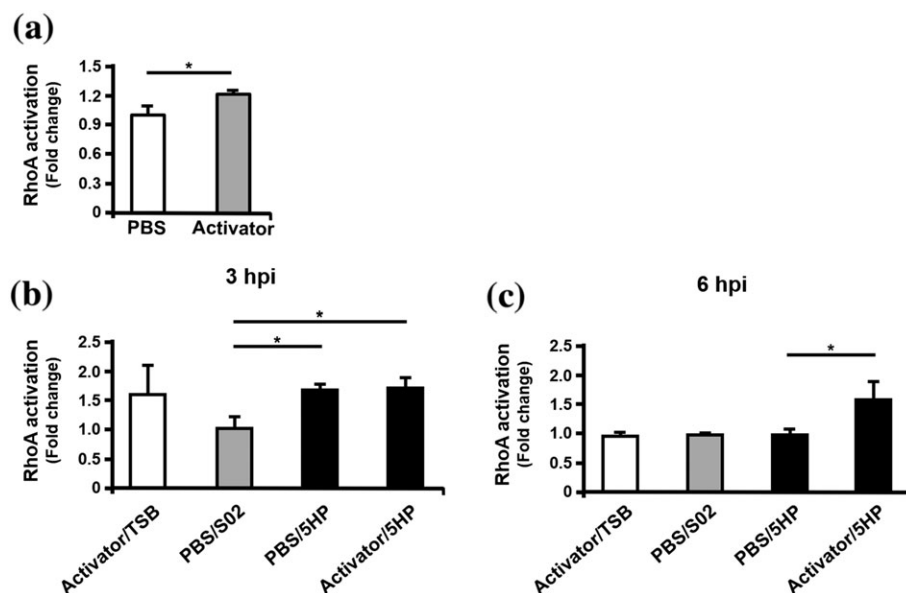


FIGURE 4 Rho activation after Rho activator pretreatment and acute hepatopancreatic necrosis disease (AHPND) infection. (a) Detection of Rho activation after Rho activator pretreatment. Stomach samples were collected at 2 hr after Rho activator injection. (b) Two hours after Rho activator or PBS pretreatment, shrimp were challenged by immersion in AHPND-causing *V. parahaemolyticus* (5HP) strain or in non-AHPND-causing *V. parahaemolyticus* (S02) or tryptic soy broth (TSB) controls. Stomach samples were collected at 3 and 6 hr after *V. parahaemolyticus* infection, and Rho activation was measured using the RhoA G-LISA activation assay. Statistically significant differences were determined by unpaired Student's *t* test ($p < .05$). hpi = hour post immersion

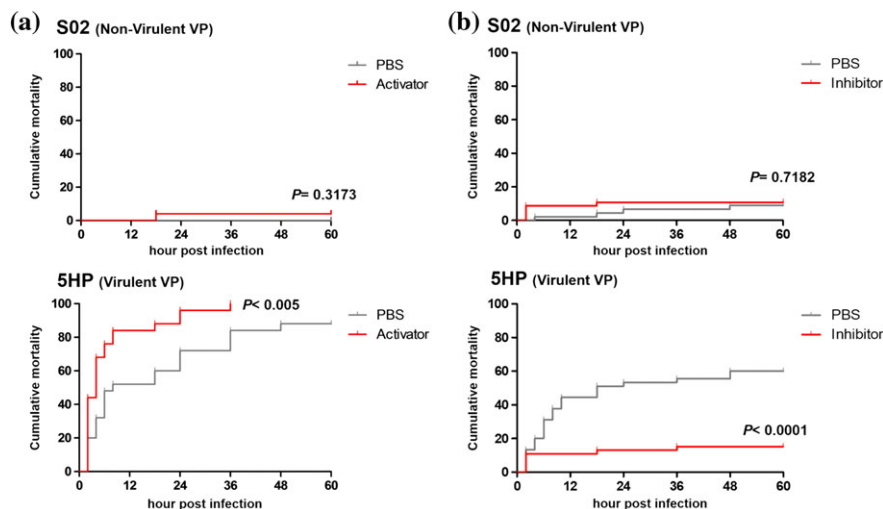


FIGURE 5 In acute hepatopancreatic necrosis disease-causing *Vibrio parahaemolyticus* (5HP)-challenged shrimp, mortality was increased after Rho preactivation and reduced after pretreatment with Rho inhibitor. Mortality rates are shown for shrimp immersed in non-acute hepatopancreatic necrosis disease-causing *V. parahaemolyticus* (S02) or 5HP after pretreatment with (a) Rho activator or (b) Rho inhibitor as indicated. Differences in mortality curves between each group were analysed by the log rank test

Rimphanitchayakit, 2017). Most of these genes are antimicrobial peptides produced by the Toll and immune deficiency pathways, which are the major innate immune pathways in shrimp (Li & Xiang, 2013). During AHPND infection, lysozymes, serine proteinase, serine proteinase inhibitors, and the prophenoloxidase system were also found to cause inflammation by activating through catalytic enzyme activity (Qi et al., 2017). In this study, many of the 376 genes that were differentially expressed in the 5HP-P group compared with the S02 group were also related to the shrimp immune systems. However, our gene ontology and pathway analysis results (Figure 1), as well as our gene-to-gene expression correlation network analysis (Figure 2), also showed that other genes of interest were involved with catalytic activity and metabolism and, in particular, with cytoskeleton regulation by Rho GTPase. As shown in

Figure 2, seven of the most strongly correlated genes were related to the Rho pathway.

Rho GTPases are common targets of pathogens as they are important nodes in eukaryotic cytoskeleton dynamics and trafficking signalling networks (Aktories, 2011; Casselli, Lynch, Southward, Jones, & DeVinney, 2008; Stones & Krachler, 2015). Human pathogenic *V. parahaemolyticus* can activate the Rho family GTPase to redistribute tight junction proteins and facilitate epithelial barrier dysfunction (Lim, Stones, Hawley, Watson, & Krachler, 2014). Our results suggest that transmigration of the AHPND-causing bacteria to the hepatopancreas likewise depends on activation of the Rho pathway, as opposed to upregulation of the Rho pathway genes. In this study, although we did not directly demonstrate that Rho activation per se could lead to an increase in cell junction width, we nevertheless

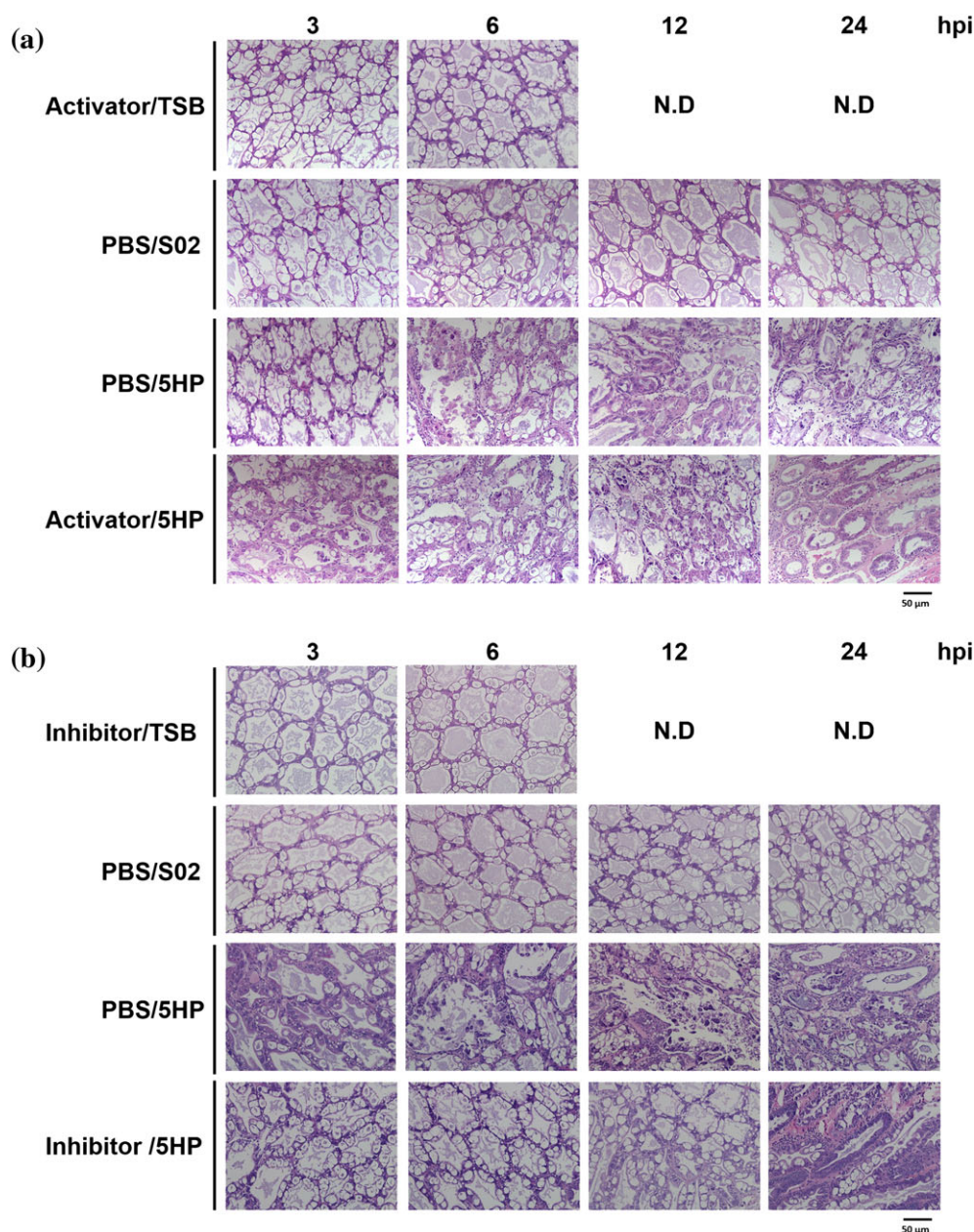


FIGURE 6 Haematoxylin and eosin-stained hepatopancreas collected from tryptic soy broth (TSB)-treated, non-acute hepatopancreatic necrosis disease (AHPND)-causing *V. parahaemolyticus* (S02)-infected, and AHPND-causing *Vibrio parahaemolyticus* (5HP)-infected groups at 0–24 hr post immersion (hpi). Normal hepatopancreas tubules are observed in the TSB-treated and S02-infected groups, whereas typical AHPND lesions with necrotic, sloughed epithelial cells were found in both of the 5HP-infected groups. However, (a) severe sloughed epithelial cells and hemocytic infiltration were observed sooner (i.e., at 3 vs. 6 hpi) in the 5HP-infected group with Rho preactivation and (b) delayed of epithelial cells sloughing and hemocytic infiltration were observed (i.e., at 6 vs. 12 hpi) in the 5HP-infected group with Rho preinhibition. Scale bar: 50 μm. N.D. = no data

found that shrimp infected with 5HP had both higher RhoA activation levels and wider cell junction gaps (Figure 3). In addition, RhoA preactivation prior to 5HP infection led to higher mortality and AHPND lesions at an earlier time point after 5HP infection; conversely, Rho preinhibition delayed AHPND infection (Figures 5 and 6). When RhoA was preactivated, pathogens and toxins were detected sooner in the hepatopancreas, whereas RhoA activation and 5HP challenge were both able to induce damage to the brush border (Figure 7).

The brush border is a covering of microvilli at the surface of the gastrointestinal epithelium (Bennett, Walker, & Lo, 2014; Mukherjee

& Wynn Williams, 1967). These microvilli are actin-filled fingerlike projections, and their integrity is often disrupted by enteric pathogens that colonise and multiply on their surface (Zhou et al., 2014). In the course of an infection, enteric pathogenic microbes often produce pili structures that tightly adhere to the microvilli on the epithelium surface, displace the luminal microbiota, hijack host signalling pathways, and disrupt the defence barrier (Ashida, Ogawa, Kim, Mimuro, & Sasakawa, 2011). The multivalent adhesion molecule 7 expressed by the human pathogenic *V. parahaemolyticus* promotes binding of the bacteria to the cell epithelial surface (Krachler, Ham, & Orth, 2011; Lim et al., 2014). This binding activates Rho signalling, which leads to

TABLE 2 Effects of Rho preactivation on AHPND infection

| | Epithelium necrosis | Hemocytic infiltration |
|---------------|---------------------|------------------------|
| 3 hpi | | |
| Activator/TSB | 0 (2) | 0 (2) |
| PBS/S02 | 0 (2) | 0 (2) |
| PBS/5HP | 1 (3) | 0 (3) |
| Activator/5HP | 2 (4) | 2 (4) |
| 6 hpi | | |
| Activator/TSB | 0 (3) | 0 (3) |
| PBS/S02 | 0 (3) | 0 (3) |
| PBS/5HP | 2 (3) | 2 (3) |
| Activator/5HP | 2 (3) | 2 (3) |
| 12 hpi | | |
| PBS/S02 | 0 (4) | 0 (4) |
| PBS/5HP | 3 (4) | 3 (4) |
| Activator/5HP | 4 (4) | 4 (4) |
| 24 hpi | | |
| PBS/S02 | 0 (3) | 0 (3) |
| PBS/5HP | 3 (4) | 3 (4) |
| Activator/5HP | 2 (5) | 1 (5) |

Note. The number indicates shrimp identified with epithelium necrosis and hemocytic infiltration, whereas a number in parentheses indicates the total number of shrimp analysed. AHPND = acute hepatopancreatic necrosis disease; 5HP = AHPND-causing *Vibrio parahaemolyticus* strain; S02 = non-AHPND-causing *Vibrio parahaemolyticus* strain; TSB = tryptic soy broth; hpi = hour post immersion.

TABLE 3 Effects of Rho preinhibition on AHPND infection

| | Epithelium necrosis | Hemocytic infiltration |
|---------------|---------------------|------------------------|
| 3 hpi | | |
| Inhibitor/TSB | 0 (4) | 0 (4) |
| PBS/S02 | 0 (4) | 0 (4) |
| PBS/5HP | 1 (4) | 0 (4) |
| Inhibitor/5HP | 0 (4) | 0 (4) |
| 6 hpi | | |
| Inhibitor/TSB | 0 (3) | 0 (3) |
| PBS/S02 | 0 (4) | 0 (4) |
| PBS/5HP | 2 (4) | 1 (4) |
| Inhibitor/5HP | 1 (4) | 0 (4) |
| 12 hpi | | |
| PBS/S02 | 0 (4) | 0 (4) |
| PBS/5HP | 2 (4) | 2 (4) |
| Inhibitor/5HP | 0 (4) | 0 (4) |
| 24 hpi | | |
| PBS/S02 | 0 (4) | 0 (4) |
| PBS/5HP | 4 (4) | 4 (4) |
| Inhibitor/5HP | 3 (4) | 2 (4) |

Note. The number indicates shrimp identified with epithelium necrosis and hemocytic infiltration, whereas a number in parentheses indicates the total number of shrimp analysed. AHPND = acute hepatopancreatic necrosis disease; 5HP = AHPND-causing *Vibrio parahaemolyticus* strain; S02 = non-AHPND-causing *Vibrio parahaemolyticus* strain; TSB = tryptic soy broth; hpi = hour post immersion.

actin rearrangement and tight junction dysfunction, and this in turn allows *V. parahaemolyticus* to transmigrate across the epithelial barrier into the blood stream (Krachler, Ham, & Orth, 2012; Lim et al., 2014; Stones & Krachler, 2015). Because *V. parahaemolyticus* is also able to attach to and colonise the midgut surface in shrimp (Soonthornchai, Chaiyapechara, Jarayabhand, Soderhall, & Jiravanichpaisal, 2015), it seems likely that 5HP may also be using the same strategy to activate Rho signalling in the host animal. This interesting possibility will need to be investigated further.

Human pathogenic *V. parahaemolyticus* uses two type 3 secretion systems, T3SS1 and T3SS2, to regulate the actin cytoskeleton. Both T3SS1 and T3SS2 produce effector proteins that regulate the Rho family GTPase, and this regulation occurs independently of the bacteria's T3SS2 toxin (Stones & Krachler, 2015; Wang et al., 2015; Yarbrough et al., 2009). The same T3SS1 system is also found in all of the published non-AHPND and AHPND strains of *V. parahaemolyticus* (Li et al., 2017). However, we show here that at least one S02 strain is unable to trigger RhoA activation (Figure 4) and disrupt barrier integrity (Figure 7). From this, we infer that even though the T3SS1 system is present, the 5HP strains might nevertheless not be using it to regulate Rho GTPase signalling in shrimp. However, because this signalling evidently occurs, and because T3SS2 is not found in the 5HP strains, we further conclude that some other, as yet unidentified factor(s) must be involved in the regulation of the Rho GTPase signalling in these virulent strains.

4 | EXPERIMENTAL PROCEDURES

4.1 | Bacterial strains

A 5HP strain and a S02 strain were isolated from Thailand and maintained on thiosulfate citrate bile salts sucrose agar. These strains were cultured in TSB medium containing 2% NaCl at 30 °C overnight before use as the bacterial inoculum for the challenge experiments.

4.2 | Experimental animals

Litopenaeus vannamei shrimp (0.2 or 2 g mean body weight) were purchased from the Center for Shrimp Disease Control and Genetic Improvement, National Cheng Kung University, and maintained in sterilised seawater (30 ppt) for at least 1 day at 27 °C before being challenged by immersion.

4.3 | Immersion challenge test

Bacterial inocula and challenge tests were conducted as described by Lai et al. (2015). Briefly, *V. parahaemolyticus* bacterial inoculum (5HP or S02) with a density of approximately 10^7 CFU/ml was prepared in TSB medium containing 2% NaCl. Each inoculum (~100 ml) was mixed with 900 ml of seawater to produce a bacteria density of approximately 10^6 CFU/ml. Control groups used 100-ml TSB

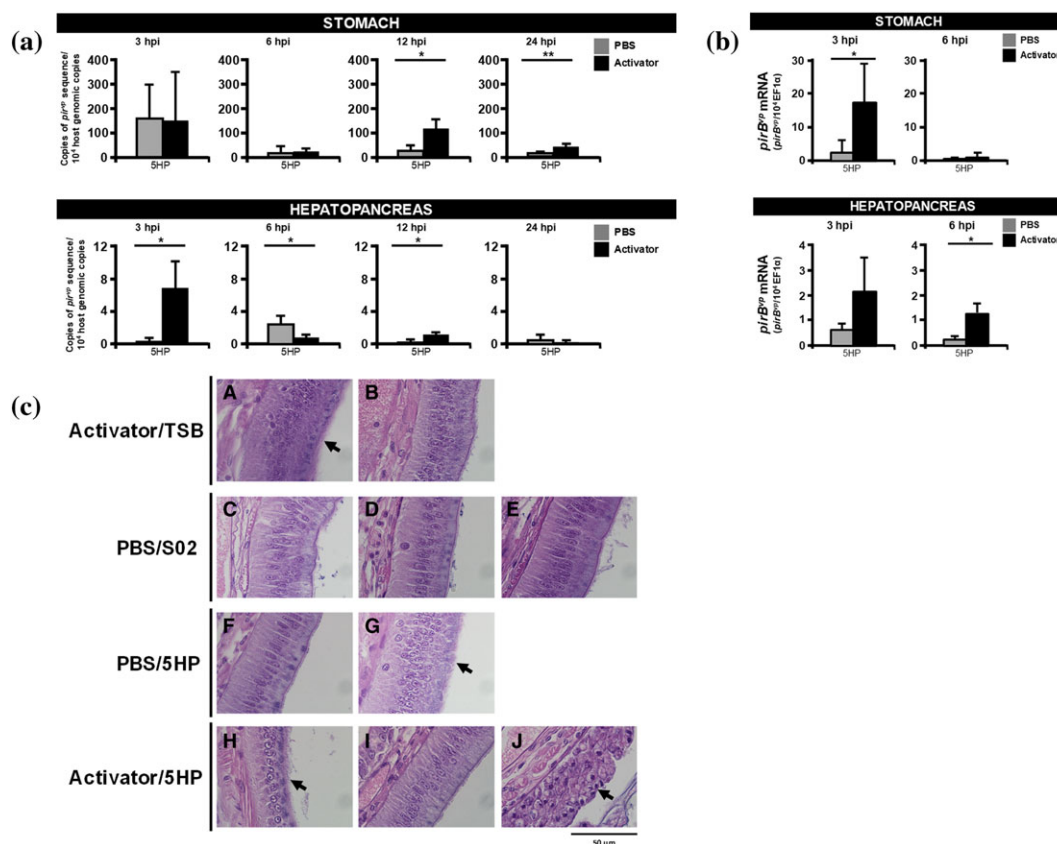


FIGURE 7 The effect of preactivation of the Rho pathway on *Vibrio parahaemolyticus* location, *pirB^{vp}* expression, and damage of the anterior midgut epithelium at 3–6 h post acute hepatopancreatic necrosis disease-causing *V. parahaemolyticus* (5HP) challenge. (a) The effect of Rho activator on the number of *pirB^{vp}* copies (genome copy number) and (b) *pirB^{vp}* mRNA gene expression in stomach and hepatopancreas at the indicate time points. Each bar represents the mean \pm standard deviation from individual shrimp samples (the number of data points shown may be less than four because any sample of statistical outlier was excluded). Statistically significant differences were determined by unpaired Student's *t* test (**p* < .05 and ***p* < .005). (c) Longitudinal section of the anterior region of the midgut, near the junction of the stomach and midgut ceca. Each histological section is from an individual shrimp sample collected at 3 hr post immersion (hpi). Black arrows indicate sections in which the brush border of the midgut epithelium has lost its integrity. TSB = tryptic soy broth

medium containing 2% NaCl in 900 ml seawater. For the experimental challenge, shrimp were immersed in one of these mixtures for 15 min, after which the shrimp and 300 ml of mixture were transferred into a shrimp tank containing 30 L of seawater. Thus, the final bacteria density in the tanks was approximately 10⁴ CFU/ml.

4.4 | RNA-Seq for transcriptomics

Shrimp stomach samples were collected from live shrimp at 24 hr and 1 week post immersion. Five individual shrimp were taken from each group at each time point. An RNeasy Mini Kit (Qiagen) was used to extract the total RNA from half of each stomach sample following the manufacturer's instructions. Quantification and quality control of the RNA samples were determined by an RNA 6000 Nano kit with Agilent 2100 Bioanalyzer (Agilent Technologies Inc.). Paired-end sequencing was performed on an Illumina NextSeq500 (Genomics BioSci & Tech Co.), and the paired-end reads were assembled using Trinity (v.2.1.1; Grabherr et al., 2011) with strand-specific mode (--SS_lib_type RF). For functional classification, annotation was determined using BLAST with the Flybase database, and analysis was conducted using PANTHER (Mi et al., 2017). For the gene-to-gene correlation network,

annotation was determined using BLAST with the NCBI-PM and EMBL-CDS databases, and analysis was conducted using the ContigViews (Liu et al., 2014) web server. Relative changes in the Rho signalling of actin cytoskeleton pathway based on KEGG was conducted using the EXPath Tool (Chien et al., 2015).

4.5 | Validation of transcriptomics data

Validation tests were conducted on some of the total RNA samples that were extracted from shrimp stomachs for the above transcriptomics analysis. These samples were subjected to real-time PCR using primer sets for eight of the defined contigs in the gene-to-gene correlation network (Table S1). EF1α was used for normalisation. Expression levels were expressed as 2^{−ΔCt}.

4.6 | Effect of AHPND infection on RhoA activation and epithelial cell ultrastructure

Shrimp (0.2 g mean body weight) were challenged as described above. Four pooled stomach samples (three shrimp in each pool sample) were collected in liquid nitrogen from each group at 3 hpi for use in the RhoA activation assays. Anterior midgut samples (~1-mm tissue

blocks) were collected from two shrimp in each group and fixed in 2.5% glutaraldehyde for TEM analysis.

4.7 | Effect of Rho activator II pretreatment on AHPND infection

Shrimp (2 g mean body weight) were intramuscularly injected with Rho Activator II (0.2 µg/g shrimp; Cytoskeleton Inc.) at the manufacturer's recommended time of 2 hr prior to immersion challenge. PBS was injected as the control. After immersion, mortality in the experimental shrimp was recorded for a period of 60 hr. Individual live shrimp samples ($n = 4$) were also taken from each group at 0, 3, 6, 12, and 24 hpi. Samples were kept either in RNA keeper (Protech Technology Enterprise Co., Ltd.) for further gene expression analysis or in liquid nitrogen for RhoA activation assays. Another set of randomly selected individual shrimp samples was fixed with Davison's fixative for histological analysis by haematoxylin and eosin (H&E) stain.

4.8 | Effect of Rho inhibitor I pretreatment on AHPND infection

Shrimp (2 g mean body weight) were intramuscularly injected with Rho Inhibitor I (0.01875 µg/g shrimp; Cytoskeleton Inc.) at the manufacturer's recommended time of 2 hr prior to immersion challenge. PBS was injected as the control. After immersion, mortality in the experimental shrimp was recorded for a period of 60 hr. Individual live shrimp samples ($n = 4$) were also taken from each group at 0, 3, 6, 12, and 24 hpi. Individual shrimp were fixed with Davison's fixative for histological analysis by H&E stain.

4.9 | Detection of *pir*^{VP} copies and *pirB*^{VP} mRNA after AHPND infection

A DNA extraction kit (GeneReach Biotechnology Corp.) was used to extract total DNA from one fourth of the same stomach samples that were used for the transcriptomics analysis. *pirB*^{VP} was then detected by PCR with the primer set PirF/PirR (Table S1) as described by Lai et al. (2015). From other shrimps, total DNA was similarly extracted from a quarter of the stomach and a quarter of the hepatopancreas. The extracted DNAs were then subjected to IQ REAL™ AHPND (GeneReach Biotechnology Corp.), which is designed on the basis of the AHPND-causing toxin genes (*pirAB*^{VP}) as published by Yang et al. (2014). To measure *pirB*^{VP} mRNA expression levels, total RNA was extracted from other quarter portions of these stomach and hepatopancreas samples with REzol reagent (Protech Enterprise). From these RNA samples, cDNA was synthesized by using a random hexamer primer (Table S1) and SuperScript™II Reverse transcriptase (Invitrogen). The cDNA was then subjected to real-time PCR with *pirB*^{VP} primers (Pir-realtime-F/Pir-realtime-R; Table S1).

4.10 | Ultrastructure observation by TEM

Anterior midgut samples for TEM observation (~1-mm tissue blocks) were fixed in 2.5% glutaraldehyde and negatively stained with uranyl

acetate. Images were captured from both TSB-treated and 5HP-infected shrimp. In five randomly selected fields (10 cell junctions) in a TSB-treated shrimp and five randomly selected fields (seven cell junctions) in a 5HP-infected shrimp, the width of each cell junction gap was measured at two locations and averaged.

4.11 | Histological analysis by H&E stain

Shrimp samples were collected as described above, and the cephalothorax was fixed with the Davison's alcohol formalin acetic acid fixative for 48 hr and subsequently replaced by ethanol for at least 24 hr using methods described by Lightner (1996). The cephalothorax was then sectioned and stained with H&E stain following standard histological methods. Hepatopancreatic and stomach epithelium structures were examined using light microscopy, and epithelium necrosis and hemocytic infiltration in the hepatopancreas were evaluated.

4.12 | RhoA activation assays

RhoA activity was detected using the RhoA G-LISA Activation Assay Biochemical Kit (kit BK124; Cytoskeleton Inc.) according to the manufacturer's instructions. Briefly, the shrimp stomach samples ($n = 4$) collected at each time point were lysed using the provided lysis buffer with protease inhibitor cocktail. Protein concentration for each sample was measured using Precision Red Advanced Protein Assay Reagent (Cytoskeleton Inc.). The lysates were diluted to 25 µg and loaded onto the G-LISA plate for 30-min incubation at 4 °C with vigorous shaking. This was followed by application of the anti-RhoA antibody and 45 min of incubation at room temperature with vigorous shaking. The signal was allowed to develop for 10 min at 37 °C. The reaction was then stopped with stop solution, and RhoA activation level was measured by absorbance at 490 nm using a microplate reader.

ACKNOWLEDGEMENTS

This study was supported financially by the Ministry of Science and Technology (MOST 106-2633-B-006-004 and MOST 106-2313-B-006-007-MY3). Two of the *Vibrio parahaemolyticus* strains, 5HP and S02, was kindly provided by Dr. Timothy W. Flegel, Dr. Kallaya Sritunyaluksana, and Dr. Siripong Thitamadee. We thank Mr. Paul Barlow, National Cheng Kung University, for his helpful criticism of the manuscript.

CONFLICT OF INTEREST

The authors declare that the research was conducted in the absence of any commercial or financial relationships that could be construed as a potential conflict of interest.

ORCID

Tze Hann Ng  <http://orcid.org/0000-0002-8260-7097>

Han-Ching Wang  <http://orcid.org/0000-0001-7283-4942>

REFERENCES

- Aktories, K. (2011). Bacterial protein toxins that modify host regulatory GTPases. *Nature Reviews Microbiology*, 9, 487–498. <https://doi.org/10.1038/nrmicro2592>

- Ashida, H., Ogawa, M., Kim, M., Mimuro, H., & Sasakawa, C. (2011). Bacteria and host interactions in the gut epithelial barrier. *Nature Chemical Biology*, 8, 36–45. <https://doi.org/10.1038/nchembio.741>
- Bennett, K. M., Walker, S. L., & Lo, D. D. (2014). Epithelial microvilli establish an electrostatic barrier to microbial adhesion. *Infection and Immunity*, 82, 2860–2871. <https://doi.org/10.1128/IAI.01681-14>
- Casselli, T., Lynch, T., Southward, C. M., Jones, B. W., & DeVinney, R. (2008). *Vibrio parahaemolyticus* inhibition of Rho family GTPase activation requires a functional chromosome I type III secretion system. *Infection and Immunity*, 76, 2202–2211. <https://doi.org/10.1128/IAI.01704-07>
- Chien, C. H., Chow, C. N., Wu, N. Y., Chiang-Hsieh, F. Y., Hou, P. F., & Chang, W. C. (2015). EXPath: A database of comparative expression analysis inferring metabolic pathways for plants. *BMC Genomics*, 16(S6). <https://doi.org/10.1186/1471-2164-16-S2-S6>
- Ge, Q., Li, J., Wang, J., Li, J., Ge, H., & Zhai, Q. (2017). Transcriptome analysis of the hepatopancreas in *Exopalaemon carinicauda* infected with an AHPND-causing strain of *Vibrio parahaemolyticus*. *Fish and Shellfish Immunology*, 67, 620–633. <https://doi.org/10.1016/j.fsi.2017.06.047>
- Grabherr, M. G., Haas, B. J., Yassour, M., Levin, J. Z., Thompson, D. A., Amit, I., ... Regev, A. (2011). Full-length transcriptome assembly from RNA-Seq data without a reference genome. *Nature Biotechnology*, 29, 644–652. <https://doi.org/10.1038/nbt.1883>
- Han, J. E., Tang, K. F. J., Tran, L. H., & Lightner, D. V. (2015). *Photobacterium* insect-related (Pir) toxinlike genes in a plasmid of *Vibrio parahaemolyticus*, the causative agent of acute hepatopancreatic necrosis disease (AHPND) of shrimp. *Diseases of Aquatic Organisms*, 113, 33–40. <https://doi.org/10.3354/dao02830>
- Kondo, H., Tinwongger, S., Proespraiwong, P., Mavichak, R., Unajak, S., Nozaki, R., & Hirono, I. (2014). Draft genome sequences of six strains of *Vibrio parahaemolyticus* isolated from early mortality syndrome/acute hepatopancreatic necrosis disease shrimp in Thailand. *Genome Announcements*, 2, e00221–e00214. <https://doi.org/10.1128/genomeA.00221-14>
- Krachler, A. M., Ham, H., & Orth, K. (2011). Outer membrane adhesion factor multivalent adhesion molecule 7 initiates host cell binding during infection by Gram-negative pathogens. *Proceedings of the National Academy of Sciences of the United States of America*, 108, 11614–11619. <https://doi.org/10.1073/pnas.1102360108>
- Krachler, A. M., Ham, H., & Orth, K. (2012). Turnabout is fair play: Use of the bacterial multivalent adhesion molecule 7 as an antimicrobial agent. *Virulence*, 3, 68–71. <https://doi.org/10.4161/viru.3.1.18172>
- Lai, H. C., Ng, T. H., Ando, M., Lee, C., Chen, I. T., Chang, S. H., ... Wang, H. C. (2015). Pathogenesis of acute hepatopancreatic necrosis disease (AHPND) in shrimp. *Fish and Shellfish Immunology*, 47, 1006–1014. <https://doi.org/10.1016/j.fsi.2015>
- Lee, C. T., Chen, I. T., Yang, Y. T., Ko, T. P., Huang, Y. T., Huang, J. Y., ... Lo, C. F. (2015). The opportunistic marine pathogen *Vibrio parahaemolyticus* becomes virulent by acquiring a plasmid that expresses a deadly toxin. *Proceedings of the National Academy of Sciences of the United States of America*, 112, 10798–10803. <https://doi.org/10.1073/pnas.1503129112>
- Li, F., & Xiang, J. (2013). Signaling pathways regulating innate immune responses in shrimp. *Fish and Shellfish Immunology*, 34, 973–980. <https://doi.org/10.1016/j.fsi.2012.08.023>
- Li, P., Kinch, L. N., Ray, A., Dalia, A. B., Cong, Q., Nunan, L. M., ... Orth, K. (2017). Acute hepatopancreatic necrosis disease-causing *Vibrio parahaemolyticus* strains maintain an antibacterial type VI secretion system with versatile effector repertoires. *Applied Environmental Microbiology*, 83, e00737–e00717. <https://doi.org/10.1128/AEM.00737-17>
- Lightner, D. V. (1996). *A handbook of shrimp pathology and diagnostic procedures for diseases of cultured penaeid shrimp*. Baton Rouge, LA: World Aquaculture Society.
- Lim, J., Stones, D. H., Hawley, C. A., Watson, C. A., & Krachler, A. M. (2014). Multivalent adhesion molecule 7 clusters act as signaling platform for host cellular GTPase activation and facilitate epithelial barrier dysfunction. *PLoS Pathogens*, 10, e1004421. <https://doi.org/10.1371/journal.ppat.1004421>
- Liu, L. Y., Tseng, H. I., Lin, C. P., Lin, Y. Y., Huang, Y. H., Huang, C. K., ... Lin, S. S. (2014). High-throughput transcriptome analysis of the leafy flower transition of *Catharanthus roseus* induced by peanut witches' broom phytoplasma infection. *Plant Cell Physiology*, 55, 942–957. <https://doi.org/10.1093/pcp/pcu029>
- Mi, H., Huang, X., Muruganujan, A., Tang, H., Mills, C., Kang, D., & Thomas, P. D. (2017). PANTHER version 11: Expanded annotation data from Gene Ontology and Reactome pathways, and data analysis tool enhancements. *Nucleic Acids Research*, 45, D183–D189. <https://doi.org/10.1093/nar/gkw1138>
- Mukherjee, T. M., & Wynn Williams, A. (1967). A comparative study of the ultrastructure of microvilli in the epithelium of small and large intestine of mice. *Journal of Cell Biology*, 34, 447–461. <https://doi.org/10.1083/jcb.34.2.447>
- Qi, C., Wang, L., Liu, M., Jiang, K., Wang, M., Zhao, W., & Wang, B. (2017). Transcriptomic and morphological analyses of *Litopenaeus vannamei* intestinal barrier in response to *Vibrio parahaemolyticus* infection reveals immune response signatures and structural disruption. *Fish and Shellfish Immunology*, 70, 437–450. <https://doi.org/10.1016/j.fsi.2017.09.004>
- Schwartz, M. (2004). Rho signaling at a glance. *Journal of Cell Science*, 117, 5457–5458. <https://doi.org/10.1242/jcs.01582>
- Soonthornchai, W., Chaiyapechara, S., Jarayabhand, P., Soderhall, K., & Jiravanichpaisal, P. (2015). Interaction of *Vibrio* spp. with the inner surface of the digestive tract of *Penaeus monodon*. *PLoS ONE*, 10, e0135783. <https://doi.org/10.1371/journal.pone.0135783>
- Soonthornchai, W., Chaiyapechara, S., Klinbunga, S., Thongda, W., Tangphatsornruang, S., Yoocha, T., ... Jiravanichpaisal, P. (2016). Differentially expressed transcripts in stomach of *Penaeus monodon* in response to AHPND infection analyzed by ion torrent sequencing. *Developmental and Comparative Immunology*, 65, 53–63. <https://doi.org/10.1016/j.dci.2016.06.013>
- Soto-Rodriguez, S. A., Gomez-Gil, B., Lozano-Olvera, R., Betancourt-Lozano, M., & Morales-Covarrubias, M. S. (2015). Field and experimental evidence of *Vibrio parahaemolyticus* as the causative agent of acute hepatopancreatic necrosis disease of cultured shrimp (*Litopenaeus vannamei*) in Northwestern Mexico. *Applied Environmental Microbiology*, 81, 1689–1699. <https://doi.org/10.1128/AEM.03610-14>
- Stones, D. H., & Krachler, A. M. (2015). Dual function of a bacterial protein as an adhesin and extracellular effector of host GTPase signaling. *Small GTPases*, 6, 153–156. <https://doi.org/10.1080/21541248.2015.1028609>
- Tran, L., Nunan, L., Redman, R. M., Mohny, L. L., Pantoja, C. R., Fitzsimmons, K., & Lightner, D. V. (2013). Determination of the infectious nature of the agent of acute hepatopancreatic necrosis syndrome affecting penaeid shrimp. *Diseases of Aquatic Organisms*, 105, 45–55. <https://doi.org/10.3354/dao02621>
- Visetnan, S., Supungul, P., Tassanakajon, A., Donpuksa, S., & Rimphanitchayakit, V. (2017). A single WAP domain-containing protein from *Litopenaeus vannamei* possesses antiproteinase activity against subtilisin and antimicrobial activity against AHPND-inducing *Vibrio parahaemolyticus*. *Fish and Shellfish Immunology*, 68, 341–348. <https://doi.org/10.1016/j.fsi.2017.07.046>
- Wang, R., Zhong, Y., Gu, X., Yuan, J., Saeed, A. F., & Wang, S. (2015). The pathogenesis, detection, and prevention of *Vibrio parahaemolyticus*. *Frontiers in Microbiology*, 6, 144. <https://doi.org/10.3389/fmicb.2015.00144>
- Yang, Y. T., Chen, I. T., Lee, C. T., Chen, C. Y., Lin, S. S., Hor, L. I., ... Lo, C. F. (2014). Draft genome sequences of four strains of *Vibrio parahaemolyticus*, three of which cause early mortality syndrome/acute hepatopancreatic necrosis disease in shrimp in China and Thailand.

Genome Announcements, 2, e00816–e00814. <https://doi.org/10.1128/genomeA.00816-14>

Yarbrough, M. L., Li, Y., Kinch, L. N., Grishin, N. V., Ball, H. L., & Orth, K. (2009). AMPylation of Rho GTPases by *Vibrio* VopS disrupts effector binding and downstream signaling. *Science*, 323, 269–272. <https://doi.org/10.1126/science.1166382>

Zhou, X., Massol, R. H., Nakamura, F., Chen, X., Gewurz, B. E., Davis, B. M., & Waldor, M. K. (2014). Remodeling of the intestinal brush border underlies adhesion and virulence of an enteric pathogen. *MBio*, 5, e01639–e01614. <https://doi.org/10.1128/mBio.01639-14>

SUPPORTING INFORMATION

Additional supporting information may be found online in the Supporting Information section at the end of the article.

How to cite this article: Ng TH, Lu C-W, Lin S-S, et al. The Rho signalling pathway mediates the pathogenicity of AHPND-causing *V. parahaemolyticus* in shrimp. *Cellular Microbiology*. 2018;20:e12849. <https://doi.org/10.1111/cmi.12849>